



Micro-PIXE, petrographic, and TL dating of Kurgesh metal slags: a recently discovered melting site in Tang-e Ma'shooreh, Lorestan

Leila khosravi¹ · Davoud Agha-Aligol²

Received: 16 May 2022 / Accepted: 12 August 2022 / Published online: 27 August 2022
© Akadémiai Kiadó, Budapest, Hungary 2022

Abstract

Western Iran, especially Lorestan has been the birthplace of metalworking technologies in different eras. The metalworking site of Kurgesh in Lorestan discovered in 2010. Here in, 16 samples using micro-PIXE technique, petrographic and TL dating, were selected and examined. The elemental composition of the slags indicates the extraction of iron in this site. Based on the results of the TL dating, the site dates back to the middle Sasanian period. Undoubtedly, the discovery of Kurgesh site can play an important role in metalworking studies of western Iran.

Keywords Slag · Micro-PIXE · TL Dating · Petrography · Kurgesh · Lorestan

Introduction

According to the obtained evidence, western Iran, especially Lorestan, has been the birthplace and the origin of metalworking technologies in different eras. Slag is the first remnant most often found in metal smelting sites. Slag is obtained from various metallurgical processes and is not a mineral or the result of the melting of natural materials. It is the product of human thought and labor to obtain raw materials in the past. Therefore, its study is particularly complex. Slag contains information about the chemical properties of all raw materials involved in a smelting process. So, its laboratory examination can be an ideal method for determining the different ore types used in the smelting process. Thus, measurement of the elemental composition and mineralogy of slag has an essential role in understanding the metallurgy and identifying the specific usage of the metal.

Archaeometric studies on old smelting slags in some cases, indicate the presence of other valuable minerals in the veins of main minerals. Therefore, the study of slag helps us to understand the technology of recovery and the extraction of metals in the ancient world. In this regard, different slag phases based on the type of extracted metals are studied and interpreted to conclude a hypothesis for how the minerals were recovered and extracted [1].

Research background and geographical location of Kurgesh site

In archeology, the study of metal works is more from an artistic perspective, and little attention has been paid to smelting and recovery methods. The iron was first identified in certain meteorites, which contained the iron in almost pure form and some nickel as an impurity. The first known iron artifacts are a few little beads obtained from two burials in Gerzeh in northern Egypt, dated to 3200 BC. These beads made from meteorite, carefully hammered, and shaped into thin plates [2].

In many cases, iron objects contain slag inclusions and remains that have changed in size and shape depending on the type of work has been done. In some studies, researchers examined metal objects using laboratory methods and instruments such as optical and electron microscopes [3, 4]. Studying and characterizing of Iranian historical iron artifacts and objects in Iran is a new topic and has received little attention regarding other metals such as

✉ Leila khosravi
l.khosravi1357@gmail.com

¹ Department of Historical Archaeology, Iranian Center for Archaeological Research (ICAR), Research Institute of Cultural Heritage and Tourism, 30th Tir Street, Tehran, Iran

² Van de Graaff Laboratory, Physics and Accelerators Research School, Nuclear Science and Technology Research Institute (NSTRI), Atomic Energy Organization of Iran, North Kargar Street, Tehran, Iran

copper alloys. But, in Europe, extensive research has been conducted to study the microstructure and corrosion of such artifacts. Philippe Dillmann et al. [3] and Neff et al. [5], both in France, have performed extensive studies and experiments on the structure of historical iron buried in the ground, to identify the form and improve the metal conditions in the face of a corrosive environment for planting nuclear waste in metal barrels [3, 5, 6].

In Iran in the early 1990s, the ancient site of Arisman, full of copper slags, was introduced to the scientific community by D. Hosseinalian, and the joint excavation of Iranians and Germans in the Arisman site [7–9]. Since then, this kind of study on iron has been carried out by a few researchers in a limited and slow process, by optical microscopic examinations of ancient iron objects obtained from archaeological excavations in Northern Iran [10, 11].

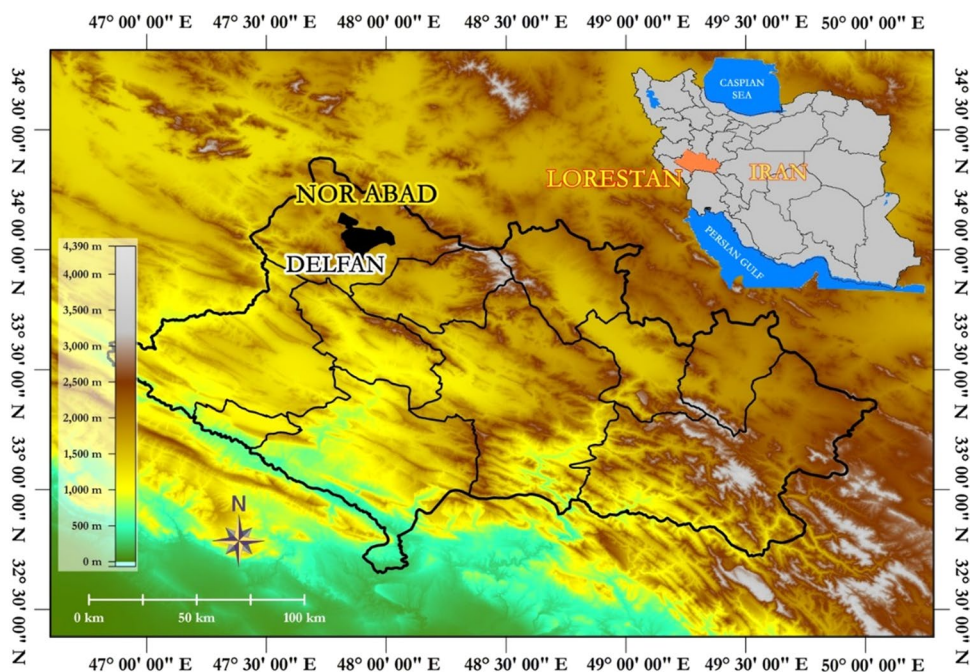
There is undoubtedly vast information in slag samples, and many questions can answer based on their examination. In this research, we generally asked the following question about metal slags obtained from the recently discovered Kurgheh site in Lorestan province: What are the characteristics of the Kurgheh slags in terms of technology and microstructure? We attempt to answer important questions in this field by using elemental analysis by the micro-PIXE technique, the petrographic method, as well as the thermoluminescence technique. Some of the questions that can answer based on the characterization and analysis of the slags are: Determining the type of extracted metal and its relationship with the applied mineral, common metalworking methods, chronology of mining activities,

specifying whether the used ore locally supplied or it imported via the commercial exchanges.

Kurgheh site (Koragah in Laki dialect means place of the furnace) located at 38 S 0762696, UTM 3749024 with a height of 1334 m above sea level, 3 km southwest of Azizkoshteh Village in Nurabad city in Delfan county, in the central district of Mirbag-e Jonubi rural district in the northwest of Lorestan province (Fig. 1). This site discovered during the archeological survey of Tang-e Ma'shooreh (Gāvshomār) and located about 60 km southwest of Delfan county in Lorestan province [12]. Tang-e Ma'shooreh is located on one of the east-to-west roads of the country. Due to its proximity to the ancient highway of Iran in the Mesopotamian plain (current road of Baghdad-Kermanshah-Hamadan), it had a significant communicative position in the past. Therefore, it recognized as the principal center for rural and urban life in different historical periods in Lorestan [13]. Before the recent survey of the area, the Holmes expedition led by Erich Schmidt in 1938, referred to the remnants of the paving of the Gāvshomār Strait (Tang-e Ma'shooreh) in their report and attributed it to the Sasanian period [14]. In 1936, Stein's expedition entered Delfan through Chegeni in the Gāvshomār Strait and went to Aleshtar from Cham-e Zakariā Village without conducting any research in this area [15]. Omran Garazhian also mentioned Gāvshomār Strait (Ma'shooreh) as No. T.G.52 in his report on the survey of Nurabad county in the fall of 1999 and the spring of 2001. But, the Kurgheh area remained hidden from all passers-by and researchers.

Kurgheh was the most significant site identified during the survey, with a pile of metal slags on its surface

Fig. 1 Geographical location of Kurgheh in Lorestan, western Iran



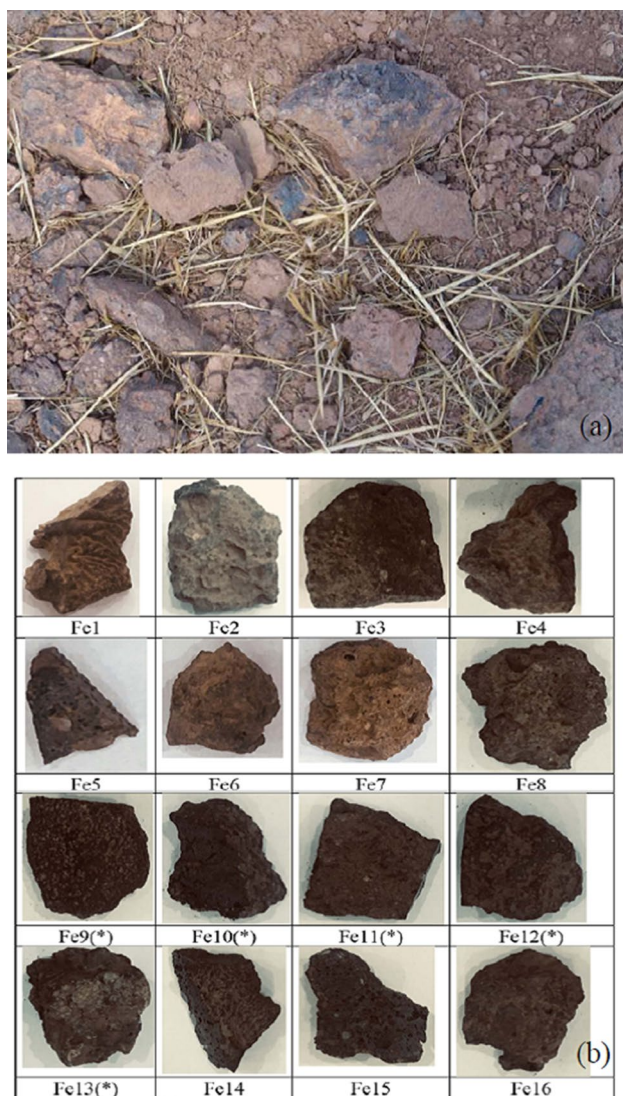


Fig. 2 **a:** a view of the surface distribution of slags in the Kurgah site, **b:** optical images of the examined metal slags from the Kurgah site by the micro-PIXE. The asterisk (*) indicates the samples analyzed by the petrographic technique

(Fig. 2a). The area has a low slope, and the closest natural features are the seasonal Zivar river in the south and the Azizkoshteh dirt road in the north. The vegetation that grows on the site and in the surrounding is wheat, oak, and pistachio trees (wild pistachios). The remarkable point about the natural landscape of the area is the presence of a seasonal river in the vicinity and the rich vegetation and shrubs around it. These trees were probably used as the fuel for smelting metal in the past. Also, in recent years, a coal mine discovered by villagers approximately 18 km from the site. Throughout the area, piles of metal slag and remnants of the kiln floor and rubble stones that belong to the architectural structures can be seen. Many floods in

consecutive years have destroyed the southern part, and plowing the land for agriculture has disturbed its surface.

Experimental

The slags of Kurgah

The samples examined in this research were obtained from the surface survey of the Kurgah site, which were collected by random sampling. From samples collection, 16 slag samples were selected to determine their elemental composition using the micro-PIXE technique. In addition, 5 samples for mineralogical examination by the petrographic technique and 3 samples for dating using the thermoluminescence technique were selected and analyzed in the laboratory of the Research Institute of Cultural Heritage. The optical images of the analyzed samples are presented in Fig. 2b.

Micro-PIXE analysis

The micro-PIXE analysis is one of the best and most accurate techniques for measuring the major and minor elements of historical and cultural samples. Micro-PIXE or Particle Induced X-ray Emission in micron-scale is a powerful technique for elemental analysis of ancient samples. In this technique, the sample is bombarded with a high-energy ion beam such as a proton beam. Due to the collision of the proton beam with the atoms of the sample, characteristic X-rays are emitted from constituent elements of the sample. The energy of these characteristic X-rays specifies the type of element and the number of X-rays with particular energy determines the concentration of elements in the examined sample [16].

In this research work, the micro-PIXE analysis was performed by the Oxford microprobe system using the 3 MV Van de Graaff accelerators at NSTRI, Tehran, Iran [17, 18]. As shown in Fig. 2, the size of the slags selected for analysis was large, and a small piece of each sample (about a few centimeters in length and width and 5 mm thickness) was carefully separated by a miniature cutter. Then, the prepared samples were fixed in resin and polished to create a smooth fresh cross-section for analysis. The samples were analyzed in a vacuum chamber using a beam of protons focused into a diameter of less than 10 μm with an energy of 2.2 MeV and a current intensity of about 50–100 pA. The characteristic X-rays were detected using a Si(Li) detector (model Sirius 80/Be) with an active area of 80 mm², a 12 μm Be window, an energy resolution of 150 eV for Fe-K α , and reversed bias of –500 V, positioned at an angle of 135° relative to the direction of the incident beam. Samples were scanned over a maximum area of 2.5 \times 2.5 mm and digitized signals were recorded in list mode using the OM-DAQ data acquisition system and the X-ray spectra were processed

using the GUPIXWIN software package [19]. To evaluate the accuracy and estimate the error in the measurement of the constituent elements in the samples, some standard samples of metal and one standard glass sample were analyzed simultaneously and under the same conditions of the samples. One-Euro coin with a nominal composition (75 wt% of copper and 25 wt% of nickel) and a tablet of a powder containing elements of copper-phosphorus-tin with a nominal composition (86 wt% of copper, 5.6 wt% phosphorus and 7.5 wt% tin) as the standard sample were analyzed and the results were compared with their nominal values. The elemental composition obtained by the micro-PIXE analysis were 74.59 wt% copper and 24.80 wt% nickel for One-Euro coin and 84.90 wt% copper, 5.71 wt% phosphorus, and 6.69 wt% tin for copper-phosphorus-tin powder tablets, respectively. Corning glass sample D as appropriate standard glass samples were also analyzed [20]. The elemental composition results of this standard sample are presented in Table 1. The elemental analysis of these standard samples and comparison of the measured value with the reported value shows that we can measure the elemental composition of historical slags with great accuracy using the micro-PIXE technique.

Petrographic technique

Among the analyzed samples by micro-PIXE, 5 samples sent to the laboratory of the Cultural Heritage for petrographic study. After cleaning the samples from waste and excess materials, polished and thin cross-sections prepared from the samples and examined under a James Swift Polarizing Microscope. The magnification used in this experiment was 4X and 10X. Since the slag, have metallic and silicate phases, it was necessary to prepare one polished and one thin cross-section from each sample, to study the silicate and metallic minerals.

Thermoluminescence dating

Among the analyzed samples by micro-PIXE, three samples were selected for thermoluminescence dating. Then these samples were prepared by fine-grain method and irradiated and measured by additive dose method. The samples were prepared, measured, and irradiated under red light to prevent any possible effect of white light on them [21].

Results and discussion

Micro-PIXE

The elemental analysis results of 16 samples of metal slag analyzed by the micro-PIXE technique were presented in terms of weight percentage and the oxide form in Table 2. To measure the elemental composition of the samples, at least two different areas on the prepared samples were analyzed to obtain the distribution map of elements, and corresponding spectra extracted to evaluate the elemental composition of the samples. Elements measured in almost all analyzed samples include magnesium oxide (MgO), aluminum oxide (Al₂O₃), silicon oxide (SiO₂), sulfur oxide (SO₃), phosphorus oxide (P₂O₅), potassium oxide (K₂O), calcium oxide (CaO), titanium oxide (TiO₂), manganese oxide (MnO) and iron oxide (Fe₂O₃). Sodium oxide (Na₂O) and chlorine (Cl) were also measured in most analyzed samples. Based on the results obtained for the elemental composition of metal slags, it is clear that the analyzed metal slags are related to iron extraction [22–24]. As shown in Table 2, the main constituents of these slags include Al₂O₃, SiO₂, CaO, MnO, and Fe₂O₃. The concentration of these elements in Table 2 shows that except for sample No.13 (Fe13), the other samples do not differ significantly in elemental composition. One of the capabilities of the micro-PIXE analysis technique is the preparation of two-dimensional (2D) distribution maps of the elements in the sample, which is done by scanning the sample by a micron-scale of the proton beam. The distribution map of the features, obtained from the analysis of metal slags shows that the distribution of elements in slags is not homogeneous, and inhomogeneity is observed in some elemental maps. Also, in almost all analyzed samples, there is a lot of porosity in the depth of the samples [23]. Figure 3 shows the elemental distribution map of few elements in sample No.2 (Fe.2). The dimension of the scan area during analysis is 2.5 × 2.5 mm. As shown in Fig. 3, the inhomogeneity of the distribution of K and Al elements throughout the surface is quite clear. We can see that these two elements are correlated. In addition, the distribution map of K and Al are uncorrelated with the other elements in the sample, which means, in the areas

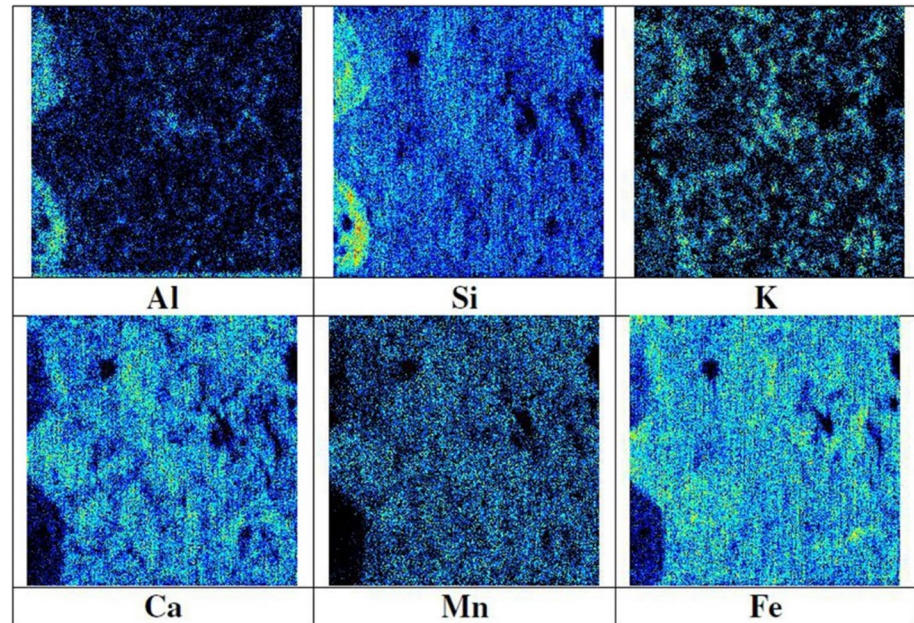
Table 1 Elemental composition of Corning standard glass sample D analyzed by the micro-PIXE, reported elemental composition of this standard sample and uncertainty of our measured value

Standard samples		Na ₂ O	MgO	Al ₂ O ₃	SiO ₂	P ₂ O ₅	SO ₃	Cl	K ₂ O	CaO	TiO ₂	MnO	Fe ₂ O ₃
Corning D	Measured value (wt%)	1.47	4.20	5.84	56.27	4.31	0.18	0.16	10.72	13.29	0.35	0.51	0.45
	Reported value (wt%)	1.20	3.94	5.30	55.24	3.93	0.30	0.40	11.30	14.80	0.38	0.55	0.52
	Uncertainty (%)	5.4	2.9	10.2	2.14	7.6	45.0	69.0	4.8	11.0	7.9	9.5	9.1

Table 2 Elemental composition and uncertainty of the measured value of metal slags analyzed by the micro-PIXE technique in oxide form and in terms of weight percentage (wt%), (nd = not detected)

Samples	MgO	Al ₂ O ₃	SiO ₂	P ₂ O ₅	SO ₃	Cl	K ₂ O	CaO	TiO ₂	MnO	Fe ₂ O ₃
Fe1	1.38±0.08	5.09±0.08	19.85±0.13	0.09±0.02	0.06±0.01	0.23±0.04	2.69±0.04	9.20±0.07	0.17±0.01	9.09±0.07	51.86±0.33
Fe2	2.13±0.12	7.08±0.12	23.89±0.16	0.13±0.03	0.08±0.02	0.03±0.01	3.36±0.05	12.78±0.10	0.25±0.02	9.59±0.08	40.25±0.25
Fe3	1.49±0.08	5.05±0.08	22.56±0.15	0.08±0.02	0.05±0.01	nd	2.93±0.05	10.36±0.08	0.20±0.02	9.83±0.08	47.33±0.30
Fe4	1.35±0.08	4.99±0.08	21.18±0.14	0.07±0.02	0.05±0.01	0.03±0.01	2.02±0.03	11.34±0.09	0.16±0.01	10.58±0.09	47.89±0.30
Fe5	1.74±0.10	6.74±0.11	23.59±0.15	0.09±0.02	0.08±0.02	0.04±0.01	3.03±0.05	10.53±0.08	0.20±0.02	8.82±0.07	44.63±0.28
Fe6	1.35±0.08	4.40±0.07	18.16±0.12	0.10±0.03	0.06±0.01	nd	2.17±0.04	8.08±0.06	0.17±0.02	2.77±0.02	62.26±0.39
Fe7	1.26±0.07	4.90±0.08	23.40±0.15	0.13±0.03	0.07±0.02	nd	3.10±0.05	8.51±0.07	0.24±0.02	8.55±0.07	49.55±0.31
Fe8	1.25±0.07	6.61±0.11	23.24±0.15	0.06±0.02	nd	nd	2.96±0.05	8.37±0.07	0.14±0.01	7.40±0.06	49.39±0.31
Fe9	2.71±0.15	10.64±0.18	26.69±0.17	0.24±0.06	0.08±0.02	0.04±0.01	3.20±0.05	22.02±0.17	0.28±0.03	7.75±0.06	25.80±0.16
Fe10	2.48±0.14	11.54±0.19	28.04±0.18	0.23±0.06	0.12±0.03	0.12±0.02	3.05±0.05	8.53±0.07	0.26±0.03	7.76±0.06	35.97±0.23
Fe11	1.84±0.10	4.69±0.08	25.44±0.17	0.12±0.03	0.06±0.01	0.04±0.01	3.29±0.05	14.28±0.11	0.19±0.02	10.07±0.08	39.30±0.25
Fe12	2.24±0.13	9.57±0.16	27.33±0.18	0.21±0.05	0.05±0.01	0.05±0.01	2.46±0.04	8.81±0.07	0.24±0.02	9.83±0.08	38.75±0.25
Fe13	1.68±0.10	9.30±0.15	66.29±0.43	0.26±0.07	0.15±0.04	0.09±0.02	4.78±0.08	6.65±0.05	0.87±0.08	0.48±0.004	9.14±0.06
Fe14	1.59±0.09	5.30±0.09	24.40±0.16	0.14±0.04	0.07±0.02	0.06±0.01	3.64±0.06	12.46±0.10	0.19±0.02	9.31±0.08	42.37±0.27
Fe15	1.63±0.09	6.30±0.10	22.86±0.15	0.19±0.05	0.11±0.03	0.05±0.01	4.11±0.07	17.47±0.14	0.24±0.02	10.57±0.09	35.40±0.22
Fe16	1.26±0.07	6.81±0.11	36.83±0.24	nd	nd	nd	2.63±0.04	12.76±0.10	0.32±0.03	4.97±0.04	34.00±0.21

Fig. 3 Distribution map of some elements in sample No. 2 (Fe2). The inhomogeneity of elements in K distribution maps in this sample is quite clear. The scan area is $2.5 \times 2.5 \text{ mm}^2$

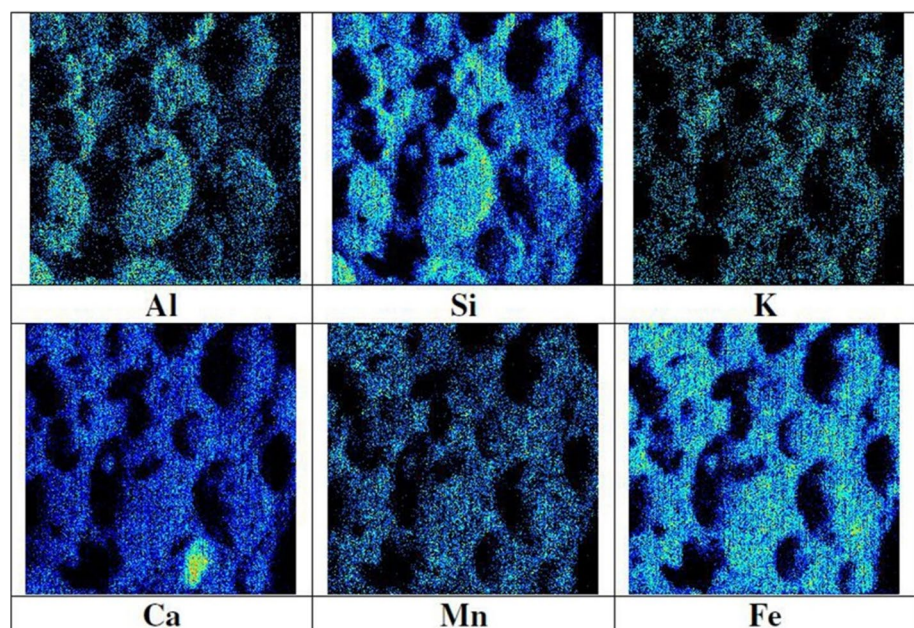


where these two elements exist, the other elements are not present, and vice versa. Moreover, in the distribution maps of elements such as Fe and Mn, some black areas are observed, which indicates the porosity of the sample [23]. These areas are scattered in the form of holes on the surface and depth of the samples. Figure 4 shows the distribution map for some elements in sample No.10 (Fe.10). This sample is completely porous, and the porosity with dark areas in the elemental distribution map is quite apparent. To understand and interpret the elemental composition of slags and to answer the questions about

determining the type of raw materials and minerals used in these metal slags, determining the extracted metal, as well as the diversity and multiplicity of primary sources used in these slags, we use bi-scatter plots based on the results of the elemental composition presented in Table 2.

The change in the weight percentage of the elements in metal slags can provide valuable information about the provenance of slags, variety, and multiplicity of raw materials used during the manufacture. It also, gives a better insight into unwanted elements that may have originated from minerals that have entered the process of extraction during the

Fig. 4 Distribution map of some elements in sample No. 10 (Fe10). The porosity in this sample is quite apparent. The scan area is $2.5 \times 2.5 \text{ mm}^2$



melting procedure of minerals [25–27]. The quality and purity of raw material sources, including iron-bearing minerals used in the slags, as well as the variety of used minerals can be determined by examining the changes in weight percentage of Fe_2O_3 in terms of elements such as SiO_2 , MnO and TiO_2 that were main impurities in iron-bearing minerals [28–30]. Figure 5a shows the changes in the weight percentage of Fe_2O_3 in terms of SiO_2 , and also in Fig. 5b the changes in the concentration of MnO in terms of SiO_2 in the analyzed slags from the Kurgeh are shown (except for Fe13 sample). As shown in Fig. 5a, the impurities of SiO_2 in these samples, varies between 17 and 40 wt%. Also, the weight percentage of Fe_2O_3 in these samples, varies between 25 and 66 wt%. In these samples, however, according to Fig. 5b, the amount of MnO varies between 7 and 11 wt% except for one samples. Therefore, as it is observed in these two figures, based on the concentration of impurities in these slags and also how these impurities change, it can conclude that the

same iron minerals with almost high purity have been used in the manufacturing process.

Also, as shown in these two figures, there is a similar trend in terms of the concentration of impurities in the slags. As shown in Fig. 5a, the amount of Fe_2O_3 in terms of SiO_2 have a relatively linear correlation between the two elements with a correlation coefficient of 0.50 ($R^2=0.50$). In addition, the value of MnO in terms of SiO_2 in the analyzed samples, which are plotted in Fig. 5b, shows a negative linear correlation between these two oxides with a correlation coefficient of $R^2=0.56$. Therefore, based on the correlation between these elements, we can conclude that in this site the minerals which metallic iron is extracted are most likely similar [27, 28].

The weight percentage of Fe_2O_3 in terms of TiO_2 , and the ratio of MnO to Fe_2O_3 in terms of the ratio of TiO_2 to Fe_2O_3 in the slags (except Fe13 sample) plotted in Fig. 6. As shown in Fig. 6a, in the analyzed samples, the concentration

Fig. 5 Changes in weight percentage of, **a** Fe_2O_3 in terms of SiO_2 , **b** MnO in terms of SiO_2 in the analyzed slags

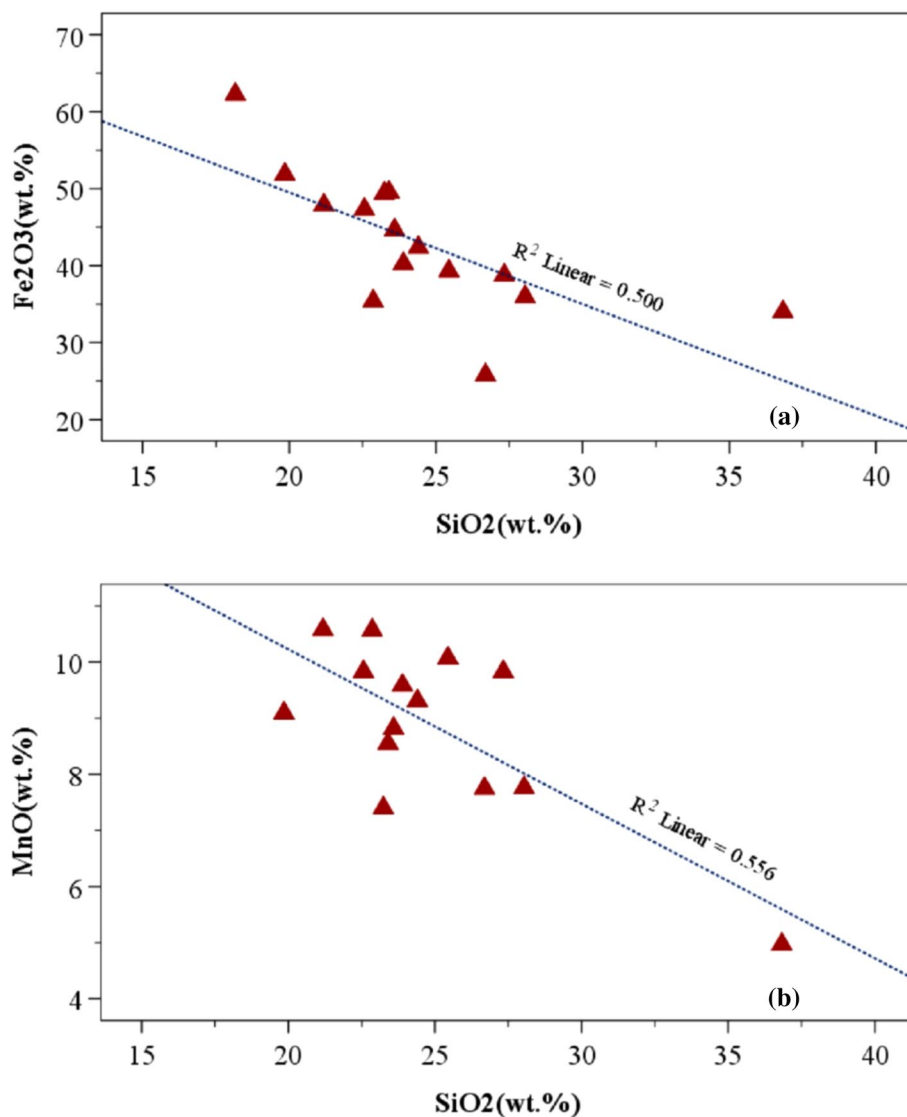
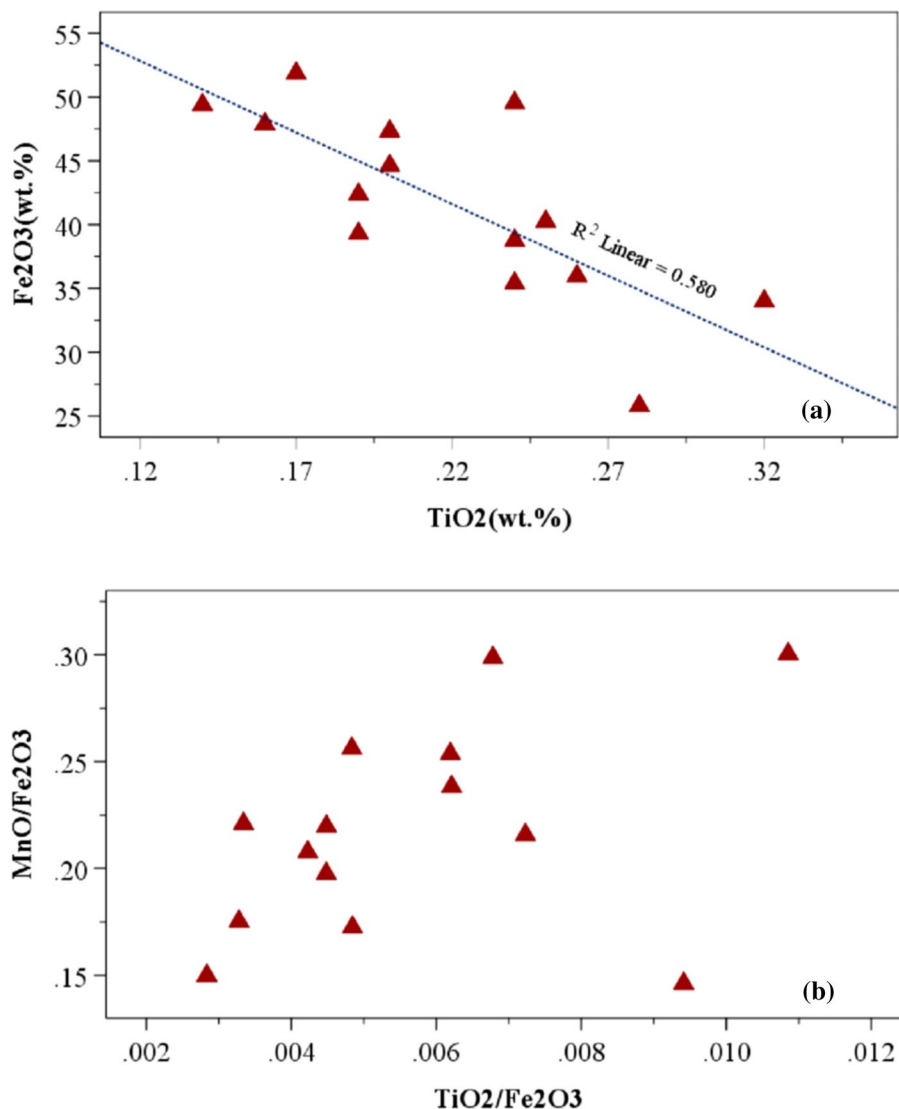


Fig. 6 **a** Changes in weight percentage of Fe_2O_3 in terms of TiO_2 , **b** changes in the ratio $\text{MnO}/\text{Fe}_2\text{O}_3$ in terms of the ratio $\text{TiO}_2/\text{Fe}_2\text{O}_3$ in the analyzed slags



of TiO_2 in terms of Fe_2O_3 in the slags, still shows a linear correlation with a correlation coefficient of 0.58 ($R^2=0.58$). Also, as demonstrated in Fig. 6b, the relative variations of MnO to Fe_2O_3 in terms of TiO_2 to Fe_2O_3 in these samples are quite small. Therefore, these little changes indicate the use of the same kind of mineral to extract iron in this historical site [24, 28]. On the other hand, the study of the elemental composition of the analyzed slags shows that in contrast to elements such as TiO_2 , MnO , Fe_2O_3 and SiO_2 , other constituents of these slags like Al_2O_3 does not correlate with elements like SiO_2 and Fe_2O_3 . Figure 7a shows the changes in weight percentage of SiO_2 in terms of Al_2O_3 , and Fig. 7b shows the changes in weight percentage of Fe_2O_3 in terms of Al_2O_3 in the slags. As shown in these two figures, based on the concentration of Al_2O_3 in these samples, almost three distinct groups can be identified. In addition, Al_2O_3 has no significant correlation with SiO_2 and Fe_2O_3 in these slags. These results indicated that aluminum impurities might not

come initially from iron-bearing ore and minerals and may have other origins. For instance, it may originate from the clay composition used in the furnace. It is also possible that three different types of minerals with variation in aluminum compounds were used during the iron extraction. According to these results, it is clear that the elemental and chemical composition of slags can be in the complex form and different compounds due to specific conditions of the melting and extracting process [26].

Petrographic analysis

A summary of the petrographic results is presented in Table 3. In the petrographic study of slags, four main categories of major minerals can be observed [31]: 1- Primary minerals that have not entered in the melting time, 2- Minerals that formed after melting, for example, during buried in the ground like olivine and pyroxene, 3- Secondary minerals,

Fig. 7 Changes in weight percentage, **a** SiO₂ in terms of Al₂O₃, **b** Fe₂O₃ in terms of Al₂O₃ in the analyzed slags

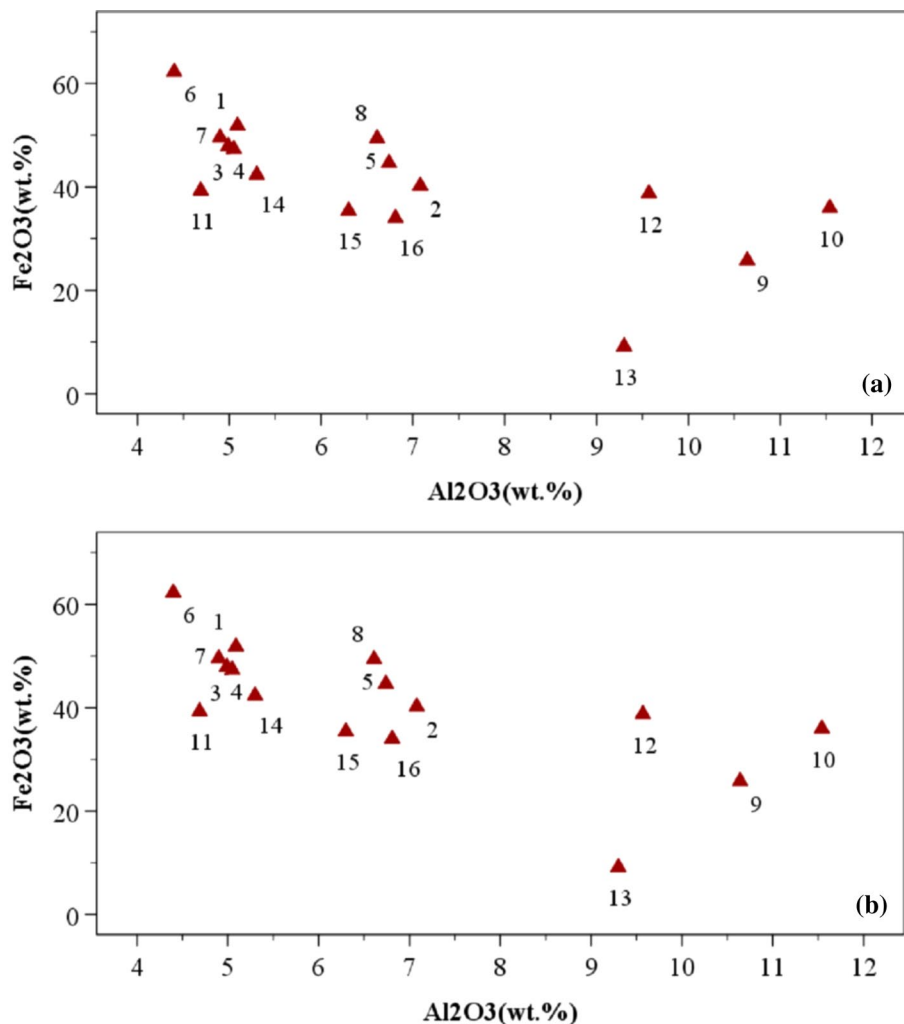


Table 3 Summary of obtained results for the 5 samples examined by the petrographic technique

Sample	Available minerals	Texture
Fe13	Primary minerals, pyroxene, metal oxide phase (opaque), secondary minerals, glass paste	Porous
Fe12	Olivine, pyroxene, metal oxide phase (opaque), glass paste	Spinifex
Fe11	Olivine, pyroxene, primary minerals, metal oxide phase (opaque), glass paste	Spinifex
Fe10	Olivine, metal oxide phase (opaque), glass paste	Spinifex
Fe9	Olivine, metal oxide phase (opaque), glass paste, secondary minerals	Spinifex

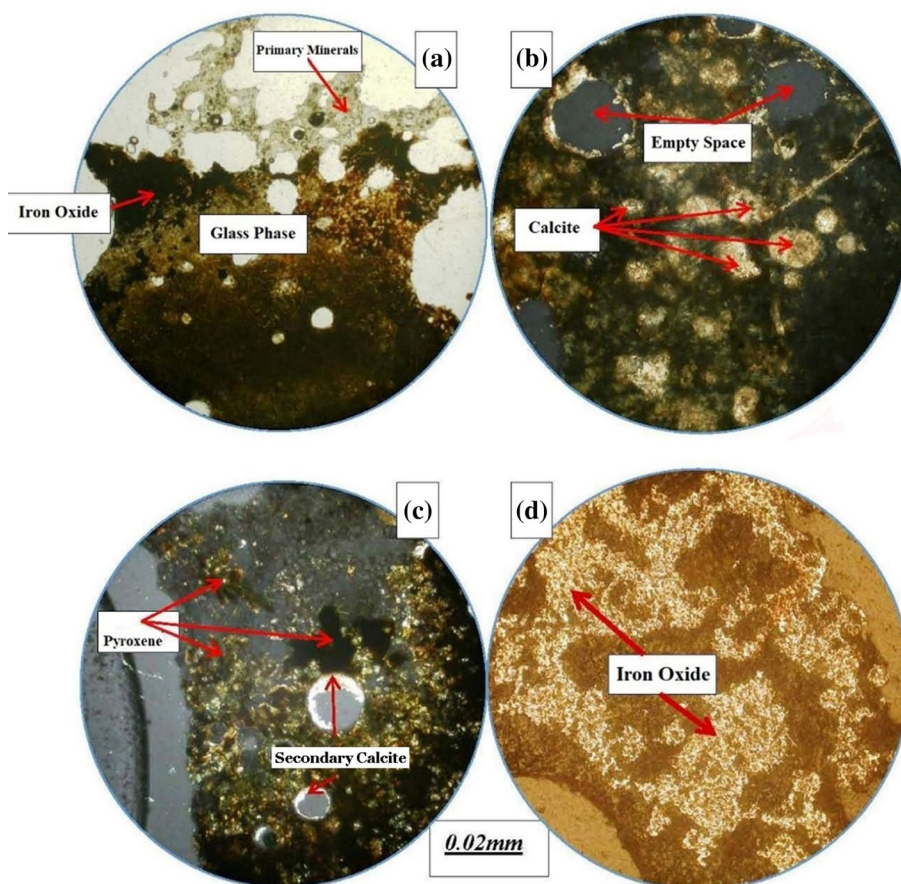
4- The metal minerals in the slags that are variable in color and they are very porous and inhomogeneous.

Sample Fe13

Minerals of sample Fe13 include primary minerals, pyroxene, glass, metal oxides (opaque), and secondary minerals. This sample is very porous and inhomogeneous. In this sample, there are remnants of primary minerals that have not entered in the melting time and generally made of silica

(Fig. 8a). Parts of the sample show greenish-yellow minerals that are black in cross light (XPL). XPL (or CPL) image is a Crossed Polarized Light image. This image captured with a polarizer under the specimen and a polarizer (analyzer) above the specimen that are crossed with each other (90°). However, PPL image is a Plain Polarized Light image. This image captured with a polarizer under the specimen and a polarizer (analyzer) above the specimen that are in-line with each other (0°). These are melted glass minerals that did not have the opportunity to crystallize due to rapid cooling.

Fig. 8 petrographic analysis results of Fe13 sample in different modes: **a**: Photomicrograph, PPL light, glass phase is seen beside dark iron oxide. Remnants of primary minerals that are generally silica is also observed, **b**: Photomicrograph, PPL light, Remnants of calcite in a dark background, which used as a melting flux. The empty space is seen dark in this light, **c**: Photomicrograph, PPL light, green pyroxene mineral beside glassy texture. Secondary calcite formed in the holes and the empty space, **d**: Photomicrograph, PPL light, polished section, iron oxide mineral in a light color. The silicate background looks dark in this light



Some opaque or dark minerals can be seen inside the glass. Remnants of limestone can be observed in this sample (Fig. 8b). The limestone is a part of the core stone or used as a melting flux to decrease the melting temperature. Furthermore, in some parts of the sample, the mineral looks green to brown. This mineral has a crystalline form and is a type of pyroxene (Fig. 8c). In this sample, some secondary minerals can be detected that formed in the soil. These minerals are of the calcite type and created by secondary processes after that the sample is placed on or under the ground and soil. To distinguish opaque minerals, a polished cross-section prepared from the slags. In reflected light, most metal minerals (opaque) are iron oxide compounds, and a small amount of pyrite (FeS_2) is seen, which indicates the recovery of iron in the studied area (Fig. 8d).

Sample. Fe12

The minerals in this sample include olivine, opaque metal oxide, and glass. The primary mineral of the silicate phase of this sample is olivine, which has the highest abundance. This mineral can be detected with a colorless, elongated, and complete crystal shape in the sample, and in the area between the opaque mineral and glass phase. The opaque mineral, found

in the form of dendrites next to the glass phase, is widespread, and dark in this sample due to the use of wood or charcoal to produce heat and carbon. In the polished section, the recovered mineral is iron oxide and iron sulfide (pyrite), which are trapped in the sample as a droplet or vesicle.

Sample. Fe11

The minerals in this sample are olivine, pyroxene, primary minerals, opaque minerals, and glass paste. The major mineral of this sample is olivine, and in the between, there is a dark green pyroxene mineral. Next to pyroxene there are iron oxide dendrites (wustite). Also, in a small amount, hematite (red iron oxide) is observed in the sample. In some parts of the sample, there are remnants of the primary mineral, which is most likely a silica compound. Iron oxide compounds are present in the polished section of the recovered mineral.

Sample. Fe10

The minerals in this sample are olivine, opaque metal oxides, and glass. Unlike sample Fe13, this sample consists of olivine crystals, which contain the most significant part

Fig. 9 Petrographic analysis results of Fe10 sample in different modes: **e**: Photomicrograph, PPL light, olivine minerals in a light color, and complete crystalline form. There are pyroxene minerals and dark-colored iron oxide between them. The empty space is seen in a light color, **f**: Photomicrograph, PPL light, olivine minerals in multi-color and complete crystalline form. Dark parts are the glass phase and opaque minerals are iron oxide

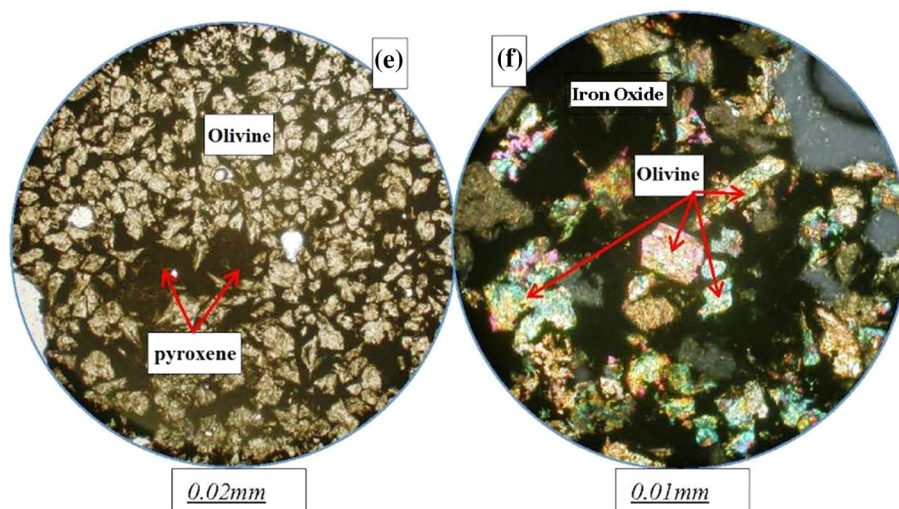


(Fig. 9e). This mineral is colorless (PPL) in light and has a complete crystalline or euhedral shape. A small amount of green pyroxene observed, next to the olivine mineral (Fig. 9f). The area between olivine and pyroxene minerals is composed of a glass phase, opaque phase and carbon minerals (Fig. 9e and f). Its dark color is caused by the recovery conditions and carbon generation during the melting of the samples. In the examined polished section, the metal mineral is recovered from iron oxide compounds (wustite) and hematite.

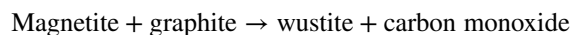
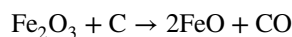
Sample. Fe9

The minerals in this sample are opaque, glass, and secondary minerals. The primary mineral of this sample is olivine, similar to the previous sample, and among this mineral is the glass phase. Next to the glass phase are iron oxide dendrites (wustite). Secondary minerals, most of which are red iron oxide compounds, are visible in this sample. Iron oxide and sulfide phase minerals detected in the polished section.

As a result of the analysis and examination of the slags, it is inferred that they were used to recover and extract metallic iron. The slag minerals can divide into three main groups. They are a group of primary minerals that have not entered during the melting time. This group of minerals is generally silicate compounds. The other group includes minerals such as olivine and pyroxene, are formed by heat. The third group are minerals that have been created after the melting process and after buried of the sample on the ground. These minerals are formed by secondary processes, such as exposure to surface water and other factors.

In the microscopic study of these samples, in addition to the mentioned minerals, some opaque minerals can be observed. Opaque minerals are found in dendritic and mass forms and are iron oxide compounds. In the polished section of the samples, the primary recovered mineral is iron. These

compounds include iron oxide (wustite) and iron sulfide (pyrite). The coexistence of the oxide and sulfide phases shows the slow casting process. Due to the presence of iron oxide in the sample, the compound of olivines is the iron-bearing type (fayalite) and iron-bearing pyroxenes of the hedenbergite, wollastonite and ferrosilite types. Remnants of stone (calcite) can be observed in some samples, which were most likely used as a melting flux. The used mineral is magnetite, which as a result of the melting process and the formation of carbon from wood firing, has caused the formation of wustite in recovering iron. The reason for the darkness of the sample is due to the presence of a high amount of carbon during the heating process and the application of wood or charcoal for producing heat:



By examining the minerals formed in the slags and the production of fayalite, it can be inferred that the temperature required for their formation is 1205 °C. This means that the furnace had a temperature of about 1205 °C. In general, the nature of slags depends on fuel compounds, furnace temperature conditions, metal compounds, and metal minerals.

Iron used as a metal in the form of artifacts produced for everyday human life. This metal is cheap compared to other options, and it is a suitable material with various manufacturing capabilities. A significant weakness of iron is its tendency to rust and corrode, [32]. Nowadays, the importance of recognizing the microstructure of iron, especially historical iron in the nuclear waste disposal industry, has garnered particular attention to this type of artifact. Studies regarding historical iron are limited [10]. The slags found in historic irons removed during the production process. These slags found around the kiln. Some of them, however, remain in the ingot and become elongated and narrow during the cold

or hot process of producing an object. Forging procedures were carried out at lower temperatures, and hammering was performed in various stages, which caused the slag to be compressed and narrowed [33].

The superimposed slag veins of the metal structure separated by the ferrite phase. The ferrite phase is characteristic of the worked iron [34]. The elongation of the slags of the worked iron depends on the method of thermomechanical formation and the direction of the work performed on the piece. If the temperature of the furnace is low and the frequency of carbon monoxide (CO) or carbon dioxide (CO₂) is limited in the furnace, the produced iron is recognized as a low carbon iron, and slag compounds are rich in iron oxide. Slags rich in iron oxide exist in the ferrite zones. The fact that metals are generally impure is essential, because the type of potential crystal growth depends very much on the purity of the metal. The hammering of the worked iron that contains impurities causes the creation of a worked microstructure in which the slags are gradually narrowed or stretched in the form of slag veins alongside the object. It is important to note that many of the inclusions in the ancient metals do not re-crystallize as a result of hot or cold work and annealing, but are shattered into smaller particles or broadened as a result of the continuation of the process [35].

Iron ore is usually a mixture of iron and large amounts of impurities such as silica or alumina (grave, sand, and clay), often present as minerals in other ores (rock clods). The iron that exists in iron ore found in the form of iron oxides. As a result of these impurities, the iron must first be removed from the rock lump, and then converted to pure iron. Iron production from quarry rock involves an oxidation and recovery reaction in the furnace mold. The top of this furnace is full of iron oxide (the most common of which is hematite (Fe₂O₃), but it can also be magnetite (Fe₃O₄), coke and limestone (CaCO₃). Iron can be recovered from its oxides at 800° C. (this temperature is significantly lower than the melting point of iron, i.e., 1535° C) [32].

TL Dating

Thermoluminescence(TL) is the process in which a thermally excited emission of the energy accumulated in a substance releases when it is heated. Some of the free carriers excited by ionizing radiation during the exposure, and some of the electrons and holes may separately capture at defects (traps). Heating may release the electrons and holes from the traps as a result of a thermally activated process, in particular, radioactively. This process is so-called TL; light emission caused by heating of a sample after illumination [36].

The TL technique can be helpful in samples containing quartz (silica) compounds that have been heated at a high temperature in the range of 800–1200 °C [29]. Three

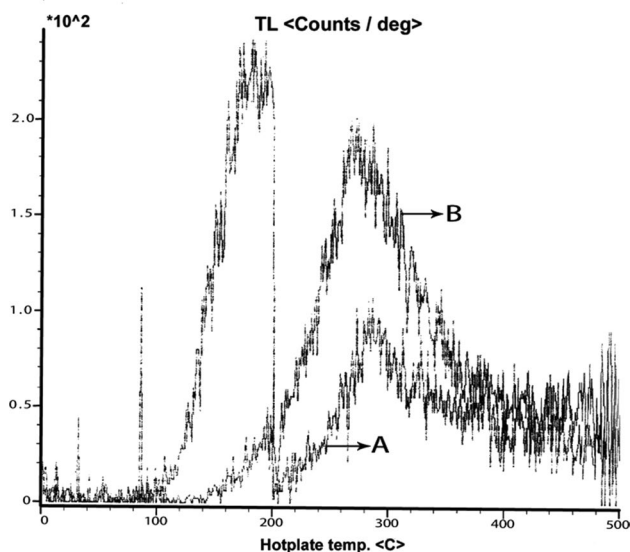


Fig. 10 A: Natural TL diagram of the sample, B: TL diagram of the sample after irradiation with a beta source, in sample Fe10

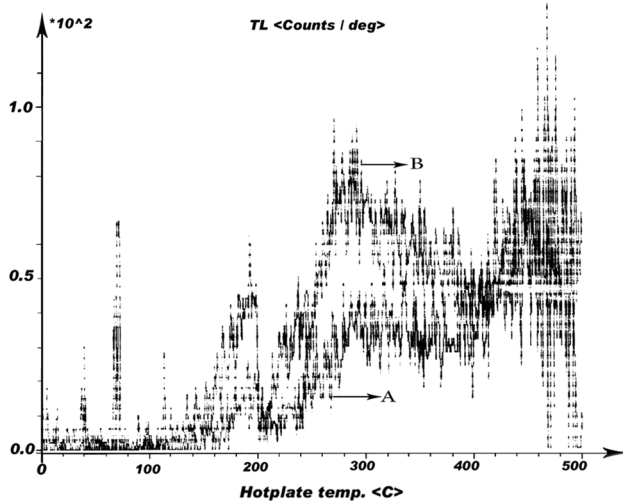


Fig. 11 A: Natural TL diagram of the sample, B: TL diagram of the sample after irradiation with a beta source, in Sample Fe12

samples were analyzed by TL technique at Conservation and Restoration of Cultural Relics of the Research Institute of Iranian Cultural Heritage (RICHT). The samples were prepared, measured, and irradiated under red light to prevent any possible effect of white light on them. The luminescence spectra obtained from the three samples are shown in Figs. 10, 11 and 12. The comparison of the Natural TL signal and TL signal after irradiation of the samples give paleo dose and the age of the samples obtained from these spectra.

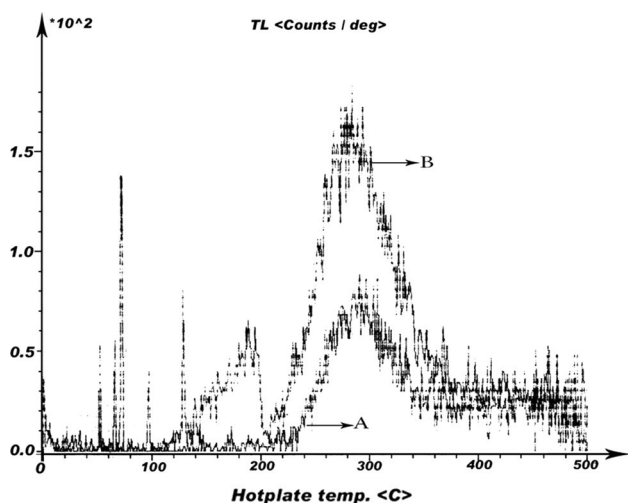


Fig. 12 A: Natural TL diagram of the sample, B: TL; diagram of the sample after irradiation with a beta source, in Sample Fe13

Fundamental principles of dating by TL technique

Natural TL signal and irradiated TL signals of the samples have been measured with TL Reader model 7188 made by ELSEC, England, in the range of 0–500 °C and with a temperature rate of 10 °C/second (Ramp Rate). After measurements and calculation of relative and absolute humidity of the samples, the dose of gamma rays and cosmic rays, the weight percentage of potassium oxide in the samples, annual dose, paleo dose, and equivalent dose, the age of samples can be calculated by using appropriate relations.

The following relations used to determine age [37]:

$$\text{Age} = \frac{\text{paleo dose}}{\text{annual dose}} \quad (1)$$

$$\text{Annual dose} = D\alpha + D\beta + D\gamma + D_C \quad (2)$$

$$\text{So, Age} = \frac{ED + I}{D\alpha + D\beta + D\gamma + D_C} \quad (3)$$

In relation (3), all parameters were defined as follow:
ED: Equivalent dose.

I = Equivalent dose in the nonlinear range.

$D\alpha$ = The amount of effective energy of alpha rays.

$D\beta$ = The amount of effective energy of beta rays.

$D\gamma$ = The amount of effective energy of gamma rays.

D_C = The amount of energy of cosmic rays transferred to the object.

Table 4 Results of the obtained and calculated effective dose of alpha, beta and gamma rays for 3 analyzed samples

Sample	$D\alpha$	$D\beta$	$D\gamma$
Fe10	31.19	3.45	1
Fe12	23.42	4.84	1
Fe13	64.74	4.27	1

Dose measurement

The samples are first treated with 5% acetic acid, then 30 tablets are prepared from each sample. For 10 tablets, after being placed in a furnace on a plate of nickel–chromium alloy in a completely pure nitrogen medium, the luminosity diagram is measured. In the next step, some tablets were irradiated with a ^{90}Sr beta source isotope at different doses. Half of the tablets measured two days after irradiation, and the other half after one month to assess how the irradiated doses lost. Next, 10 tablets measured by a ^{241}Am isotope source with different radiation doses. By measuring them, the adequate amount of alpha beam energy and the sensitivity of the sample to the alpha beam are determined. By comparing the initial radiation diagram (standard TL diagram of the sample) and the radiation diagram of the part irradiated with beta ray, the dose received in each sample or the equivalent dose is calculated [21].

Determination of the concentrations of radionuclide elements in the sample

Natural uranium isotopes (^{235}U and ^{238}U), and ^{232}Th concentrations were measured by the alpha counting method. Furthermore, in determining the concentration of U and Th elements by lateral measurement, the non-emission of radon gas in the samples has been investigated.

Also, ^{40}K concentration was measured by flame photometry in a chemistry laboratory. In this method, melting of the samples was done by using an electric furnace (CWF 1200 model) and with the chemical substance sodium lithium metaborate. The potassium percentage of the samples was calculated by using a flame spectrometer (Flame photometer 410). It is worth mentioning that in the final calculations, the amount of potassium dioxide is included in the effective amount of beta rays. The concentration of radionuclide of K, Th, and U was used to calculate the annual dose.

The Results of the calculated effective dose of alpha, beta and gamma rays for 3 analyzed were presented in Table 4. In fact, the age calculated from the above relationships have been a while since the minerals in the clay were last heated to over 400 °C. The obtained date is calculated in terms of one year equal to 365 days and is presented in Table 5. It means that, we subtract the obtained amount from the present time until the desired year is obtained. The error and

Table 5 TL dating results for 3 slag samples

Sample	Depth	Percentage of potassium oxide (K ₂ O%)	Thorium concentration (ppm)	Uranium concentration (ppm)	Error in age (%)	Age
Fe10	Superficial	1.48 ± 0.15	2.45 ± 0.24	3.50 ± 0.35	4.79	1670 ± 80 years ago
Fe12	Superficial	1.71 ± 0.17	3.75 ± 0.37	3.24 ± 0.32	6.86	1640 ± 100 years ago
Fe13	Superficial	1.216 ± 0.12	6.10 ± 0.61	6.59 ± 6.59	7.49	1690 ± 120 years ago

uncertainty in calculated age and concentration of Th, U and K is about 10 percent [38].

TL results suggest the dating of the middle Sasanian period for this site. The Sasanian period is one of the most glorious eras in the history of Iran. The study of artistic and military works of this period shows that the knowledge of casting and production of metal artifacts was of exceptional importance and had made significant progress. Although these artifacts have been investigated often based on visual characteristics and less attention has been paid to the methods of melting and recovery. Metalworking in the Sasanian period experienced by a large group of artists, which can be directly related to the significant reduction in the number of rock reliefs in Iran. The manufacture date of most metal objects in the Sasanian period is related to the sixth and seventh centuries AD, when art was entirely, out of the monopoly of the royal court and its themes were also diversified [39].

Conclusions

In this research work, considering the common metalworking methods, determining the chronology of mining activities, and identifying that the used ore was locally supplied or imported via the commercial exchanges were performed by different laboratory techniques on several samples from Kurgah. By studying and examining the slags, it concluded that they used to recover iron. Elemental composition of slags based on the amount of impurities in these slags and also how these impurities change, it can be concluded that the same iron minerals with almost high purity have been used in the manufacturing process. Based on Petrographic analysis, three main mineral groups were identified in the slags. In addition, some opaque mineral, which include an iron oxide compound found in dendritic and mass form. The coexistence of the oxide and sulfide phases shows the slow casting process.

Remnants of calcite can detect in some samples, most likely used as a melting flux. The applied mineral is magnetite, which due to the melting process and the formation of carbon from wood firing, has caused the formation of wustite in recovering iron. In addition, by examining the minerals formed in the slags and the production of phyllite,

it is inferred that the temperature required for its formation is 1205° C. This means, the furnace had a temperature range of 1205 to 1300 degrees. The nature of slags depends on the fuel compounds, furnace temperature conditions, metal compounds, and metal minerals. Indeed, the ancient metalworkers engaged in metalworking where the mines of those metals and the required fuel were in the vicinity. The rich vegetation and coal mines in the area have made it possible to melt metals in this site. The experimental results show that the slags made of iron. This is a significant discovery, because tin and copper sources have been proven so far, but this has not yet been well established for iron.

TL results suggest the dating of the middle Sasanian period for this site. The Sasanian period is one of the most glorious periods in the history of Iran, and the study of the objects of this period shows that the knowledge of casting and manufacturing of metal artifacts was of exceptional importance. Although, the study of these artifacts has mostly been from an artistic perspective and less attention has been paid to the methods of melting and recovery. The discovery of the Kurgah site will undoubtedly have valuable results. Conducting extensive research and studies on the metalworking process in this area of Iran can also use to study the cultural, economic and social developments of the region in the historical period.

Declarations

Conflict of interest The authors declare that they have no known competing financial interests or personal relationships that could have appeared to influence the work reported in this paper.

References

1. Emami SMA (2005) The importance of mineralogical studies on old smelting slags in the paragenesis of metal ores. In: Iranian Mining Engineering Conference, University of Tarbiat Modares, 20–22 January: pp 1–15
2. Rehren T, Belgya T, Jambon A, Kali G, Kasztovszky Z, Kis Z, Kovacs I, Maroti B, Torres MM, Miniaci G, Pigott VC, Radivojevic M, Rosta L, Szentmiklosi L, Szokefalvi-Nagy Z (2013) 5,000 years old Egyptian iron beads made from hammered meteoritic iron. *J Archaeol Sci* 40:4785–4792

3. Dillmann P, Balasubramaniam R, Beranger G (2002) Characterization of ancient Indian iron and entrapped slag inclusions using electron, photon and nuclear microprobes. *Bull Mater Sci* 24(3):317
4. Pingitore G, Cerchiara T, Chidichimo G, Castriota M, Gattuso C, Marino D (2015) Structural characterization of corrosion product layers on archaeological iron artifacts from Vigna Nuova, Crotona (Italy). *J Cult Herit* 16:372–376
5. Neff D, Dillmann P, Bellot-Gurlet L, Beranger G (2005) Corrosion of iron archaeological artefacts in soil: characterisation of the corrosion system. *Corros Sci* 47(2):515–535. <https://doi.org/10.1016/j.corsci.2004.05.029>
6. Neff D, Dillmann P, Descostes M, Beranger G (2006) Corrosion of iron archaeological artefacts in soil: estimation of the average corrosion rates involving analytical techniques and thermodynamic calculations. *Corros Sci* 48(10):2947–2970. <https://doi.org/10.1016/j.corsci.2005.11.013>
7. Hosseinalian D (2000) Report on the first season of excavations at Arisman. *Ketabe Mahe Honar* 20–21:65
8. Stollner T (2004) Early mining and metallurgy on the Iranian plateau. *Katalog der Ausstellung des Deutscher Bergbau-Museum Bochum in Verbindung mit der Iranischen Kulturerbe Organisation (ICHO), vom 28.11.2004 bis 28.05.2005* Herausgegeben :193–207, Bochum
9. Chegini N, Helwing B, Parzinger H, Vatandoust A (2004) Pre-historic industrial settlement on the Iranian Plateau – Research at Arisman Persiens Antike Pracht”, *Katalog der Ausstellung des Deutscher Bergbau-Museum Bochum in Verbindung mit der Iranischen Kulturerbe Organisation (ICHO), vom 28.11.2004 bis 28.05.2005* Herausgegeben: 210–217, Bochum
10. Jaffari A, Odehbash O, Abedini Iraqi M (2017) The Microscopic studies on the ancient iron objects from archaeological excavation of the North of Iran. *Pazhohesh-Ha-Ye Bastanshenasi Iran* 15(7):131–147
11. Salem Y, Oudbashi O, Eid D (2019) Characterization of the microstructural features and the rust layers of an archaeological iron sword in the Egyptian Museum in Cairo (380–500 A.D.). *Herit Sci*. <https://doi.org/10.1186/s40494-019-0261-2>
12. Khosravi L (2010) Archaeological survey and reconnaissance report of Tang-e Ma'shooreh Dam in Lorestan. *Archives of the Iranian Center for Archaeological Research*, Tehran
13. Izadpanah H (2005) Lorestan in the passage of time and history. *Asatir Publication*, Tehran
14. Chegini N (1993) The holmes expedition: The first archeological activities in Lorestan. *Majale Bastanshenasi va Tarikh* 1–2(13–14):97–114
15. Stein A (1940) *Old routes Western Iran*. Macmillan and Co, London
16. Nastasi M, Mayer J, Wang Y (2014) *Ion beam analysis: fundamentals and applications*. CRC Press, Boca Raton
17. Grime GW, Watt F (1988) Focusing protons and light ions to micron and submicron dimensions. *Nucl Instrum Methods Phys Res Sect B* 30:227–234
18. Tayyari J, Emami MA, Agha-Aligol D (2021) Identification of microstructure and chemical composition of a silver object from Shahrak-e Firouzeh, Nishapur. *Iran, Surfaces and Interfaces* 25:101168
19. Campbell JL, Boyd NI, Grassi N, Bonnicksen P, Maxwell JA (2010) The Guelph PIXE software package IV. *Nucl Instrum Methods Phys Res Sect B* 268:3356–3363
20. Vicenzi EP, Eggins S, Logan A, Wysoczanski R (2002) Microbeam characterization of corning archeological reference glasses: new additions to the smithsonian microbeam standard collection. *J Res Natl Inst Stan Technol* 107(6):719. <https://doi.org/10.6028/jres.107.058>
21. Bahroloulomi F (2015) Final report on thermoluminescence dating results of slags of Koragah Lorestan. Tehran, Research Center for Conservation of Cultural Relics (RCCCR)
22. Ilani S, Ledermanb Z, Bunimovitz S (2020) Iron oxide concretions as raw material for iron IIA iron metallurgy in the southern Levant: new evidence from Tel Beth-Shemesh. *Isr J Archaeol Sci Rep* 34:102570
23. Stepanov IS, Weeks L, Franke KA, Overlaet B, Alard O, Cable Charlotte M, Al Aali YY, Boraik M, Zein H, Grave P (2020) The provenance of early Iron Age ferrous remains from south-eastern Arabia. *J Archaeol Sci* 120:105192
24. Zoua G, Minb R, Cuic J, Mac R, Zhouc X, Yang C (2019) The special iron making in Southwest China around the 10th CE: scientific evidence from an iron smelting site in Erhai lake area, Yunnan province. *J Cult Herit* 37:266–272
25. Portillo H, Zuluaga MC, Ortega LA, Alonso-Olazabal A, Murelaga X, Martinez-Salcedo A (2018) XRD, SEM/EDX and micro-Raman spectroscopy for mineralogical and chemical characterization of iron slags from the Roman archaeological site of Forua (Biscay, North Spain). *Microchem J* 138:246–254
26. Buchwald VF, Wivel H (1998) Slag analysis as a method for the characterization and provenancing of ancient iron objects. *Mater Charact* 40:73–96
27. Miono S, Zheng C, Nakayama Y, Manabe S, Ohmichi K (1996) Search for the origin of iron manufacturing at Kansai area in Japan by PIXE analysis. *Nucl Inst Methods Phys Res B* 109(110):677–680
28. Girbal B (2019) Late iron age sunken-shaft smelting sites in Kent – analysis of the Iron working waste from Stockbury. *J Archaeol Sci Rep* 27:101930
29. Hagihara N, Miono S, Chengzhi Z, Nakayama Y, Hanamoto K, Manabe S (1999) The combined application of PIXE analysis and thermoluminescence (TL) dating for elucidating the origin of iron manufacturing in Japan. *Nucl Inst Methods Phys Res Sect B* 150:635–639
30. Paynter S (2006) Regional variations in bloomery smelting slag of the iron age and romano-british period. *Archaeometry* 48(2):271–292
31. Beheshti I (2016) Final Report on Petrographic Results of Slags of Kouragah Lorestan. Tehran, Research Center for Conservation of Cultural Relics (RCCCR)
32. Scott D, Eggert G (2009) *Iron and steel in art, corrosion colorant, conservation*. Archetype Publication, London
33. Bachmann HG (1982) *The Identification of Slag from Archaeological Sites*. Occasional Publication, No. 6. the Institute of Archaeology, London
34. Barrena MI, Gomez de Salazar JM, Soria A (2008) Raman Iron axes manufacturing technology. *Departamento de Ciencia de los Materiales, Facultad de Ciencias Quimicas, Universidad Complutense de Madrid*, 28040 Madrid, Spain. *Nucl Instrum Methods Phys Res B* 266:955–960
35. Scott DA (1991) *Metallography and microstructure of ancient and historic metals*. The Getty Conservation Institute
36. Komarova Ya M, Aluker NL, Bobrov VV, Sorokina NV (2011) Thermoluminescent dating of archaeological pottery. *Inorg Mater* 47(5):614–618
37. Aitken MZ (1985) *Thermoluminescence Dating*. Academic Press, London
38. Bahroloulomi F (2013) *Dating methods in archaeology*. Samt Press, Tehran
39. Akhavan MN (2012) Praise of life as Zoroastrian belief in Sassanid metal containers. *Kimiya-ye-Honar The Quarterly Periodical of the Advanced Research Institute of the Arts*. 1, 2nd, pp 15–30

Publisher's Note Springer Nature remains neutral with regard to jurisdictional claims in published maps and institutional affiliations.

Springer Nature or its licensor holds exclusive rights to this article under

a publishing agreement with the author(s) or other rightsholder(s); author self-archiving of the accepted manuscript version of this article is solely governed by the terms of such publishing agreement and applicable law.